metals

MDPI

Article

Thermophysical Properties of the $Fe_{48}Cr_{15}Mo_{14}C_{15}B_6Y_2$ Alloy in Liquid State

Dmytro S. Kozak [1,2], Vladimir S. Tsepelev [2], Viktor V. Konaskov [2], Viktor V. Vyukhin [2], Vladislav Y. Zadorozhnyy [3], Andrey I. Bazlov [4,5], Askar R. Kvaratskheliya [3,*], Andrey A. Tsarkov [4] and Jan F. M. Van Impe [1]

1 Chemical and Biochemical Process Technology and Control (BioTeC+), Department of Chemical Engineering, KU Leuven/Campus Gent, 9000 Leuven, Belgium; dmytro.kozak@kuleuven.be (D.S.K.); jan.vanimpe@kuleuven.be (J.F.M.V.I.)
2 Research Centre for Metallic Liquids Physics, Ural Federal University (UrFU), 19 Mira Street, 620002 Yekaterinburg, Russia; v.s.tsepelev@urfu.ru (V.S.T.); vvk98005@gmail.com (V.V.K.); v.v.vyukhin@urfu.ru (V.V.V.)
3 College of New Materials and Nanotechnologies, National University of Science and Technology (MISIS), Leninsky Prosp. 4, 119049 Moscow, Russia; zadorozhnyyvlad@gmail.com
4 College of Environmentally Sound Technologies & Engineering, National University of Science and Technology (MISIS), Leninsky Prosp. 4, 119049 Moscow, Russia; bazlov@misis.ru (A.I.B.); tsarkov.aa13@gmail.com (A.A.T.)
5 Russia and Research Laboratory for Mechanics of Advanced Bulk Nanomaterials for Innovative Engineering Application, St. Petersburg State University, 7/9 Universitetskaya nab., 199034 St. Petersburg, Russia
* Correspondence: a.r.kvarts@gmail.com

Citation: Kozak, D.S.; Tsepelev, V.S.; Konaskov, V.V.; Vyukhin, V.V.; Zadorozhnyy, V.Y.; Bazlov, A.I.; Kvaratskheliya, A.R.; Tsarkov, A.A.; Van Impe, J.F.M. Thermophysical Properties of the $Fe_{48}Cr_{15}Mo_{14}C_{15}B_6Y_2$ Alloy in Liquid State. *Metals* **2021**, *11*, 823. https://doi.org/10.3390/met11050823

Academic Editor: Qingping Cao

Received: 31 March 2021
Accepted: 7 May 2021
Published: 18 May 2021

Abstract: In this work, the physical properties of $Fe_{48}Cr_{15}Mo_{14}C_{15}B_6Y_2$ alloy in liquid state at high temperature are studied. It was observed that the basic physical characteristics of the alloy, such as viscosity, electrical resistivity, and density, decrease with an increase of the temperature to 1700 °C. An abnormal increasing rate of viscosity for $Fe_{48}Cr_{15}Mo_{14}C_{15}B_6Y_2$ alloy in the temperature range from 1360 to 1550 °C was noted. The measurement of the electrical resistivity and density did not reveal any anomalies in the same temperature range.

Keywords: viscosity; electrical resistivity; density; microstructure

1. Introduction

Interest in the synthesis and mechanical characterisation of Fe-based bulk amorphous alloys, also known as bulk metallic glasses (BMGs), started in the early 1990s [1–3]. These amorphous alloys have been shown to have a number of enhanced properties, such as superior mechanical properties and improved corrosion resistance [4–7]. Moreover, the soft magnetic properties of the Fe-based alloy led to widespread use of the material. An Fe-based amorphous alloy that has attracted a lot of attention in recent years is $Fe_{48}Cr_{15}Mo_{14}C_{15}B_6Y_2$, with several recent studies delving into its structural, mechanical, physical, and chemical properties [8–10]. However, the glass-forming ability (GFA) of Fe-based BMGs is the main limiting factor that has prevented their extensive use as structural and functional materials.

In the last few decades, studies on Fe-based BMGs have shifted their focus to their liquid state (metallic melts) [11,12]. This is due to the fact that the dynamical processes in liquids and how liquids transform to glasses are major outstanding questions in condensed matter science [13–15]. Furthermore, such information is essential to understand the glass-forming ability of the alloys containing rare elements and boron [16–21]. One typical example is the strong influence that was observed between the casting temperature and the critical sample diameter for the $Fe_{50}Cr_{15}Mo_{14}C_{15}B_6$ alloy [22].

One of the temperature-sensitive parameters of such alloys in the liquid state is viscosity. This characteristic is crucial in revealing changes in the liquid state as the sample is heated or cooled. Nowadays, various techniques are applied to measure the viscosity of metallic melts, including parallel plate rheometry [23], tensile creep [24] penetration viscometer [25,26], and the bending beam test [27–29].

There are other methods for studying the behaviour of metallic melts, which include the measurement of density, surface tension, and electrical resistivity in the liquid state across a range of temperatures. These methods can give a general idea on how physical properties of the metallic melt change at various temperatures. However, it should be noted that the physical properties of metallic melts at high temperatures are significantly dependent on the chemical composition [22].

In recent years, various mathematical models have been developed to predict the properties of melts. However, it has been shown that such models are not able to predict the properties of multicomponent melts with sufficient accuracy [14]. Thus, the development of new alloys and technologies is still dependent on experimental data. In light of this, the main aim of the present research is to study the physical properties of the $Fe_{48}Cr_{15}Mo_{14}C_{15}B_6Y_2$ alloy (viscosity, density, and electrical resistance) in a liquid state and to reveal changes in the physical properties during heating and cooling cycles.

As a result we obtained bulk amorphous-crystalline alloy and provided its viscosity measurements in the liquid state.

2. Materials and Methods

2.1. Alloy Preparation and Structure Characterisation of Samples

$Fe_{48}Cr_{15}Mo_{14}C_{15}B_6Y_2$ (atomic % compositions) alloy ingots were prepared by induction-melting a mixture of the commercial-grade pure elements in the required proportions (minimum purity of each element used was 99.9 wt.%). Then, the ingots were melted again and injected through a nozzle into a copper mould to produce ingots with a diameter of 12 mm. It should be noted that to achieve volumetric amorphization of the $Fe_{48}Cr_{15}Mo_{14}C_{15}B_6Y_2$ alloy, the ingot diameter should not exceed 7 mm [30]. However, in this study, the ingot diameter for this alloy was deliberately set to 12 mm, in order to obtain ingots having both crystalline and amorphous phases.

The samples were first polished and then etched by using 25% aqueous HNO_3. The resulting microstructure was then observed by a scanning transmission electron microscope (Tescan Vega 3 LMH, TESCAN ORSAY HOLDING, Brno, Czech Republic) operated at 20 kV, in back-scattered electron mode.

A Vicker's test (Thixomet SmartDrive MHT, Thixomet, St.-Petersburg, Russia) was also performed using a pyramidal diamond indenter to measure the microhardness of individual phases in the structure of the alloy under a load of 0.98 N. An X-ray diffraction (XRD) analysis was also carried out by using Bruker AXS GmbH (Bruker, Billerica, MA, USA) apparatus with a monochromatic Cu*Ka* radiation at the accelerating voltage of 30 kV and a current of 30 mA. The percentage of the amorphous phase was determined by using a kinematic standard method [31] and annealed nickel powder as a standard.

2.2. Differential Scanning Calorimetry Measurement

The thermal properties of the glassy alloys were measured using a Setaram Labsys differential scanning calorimetry (DSC, Setaram Instrumentation, Caluire-et-Cuire, France) instrument under an Ar gas flow, in Al_2O_3 crucible. The measured temperatures ranged from room temperature to 1340 °C with the heating rate 20 °C/min. The mass of the samples was 10–15 mg.

2.3. Measurement of the Kinematic Viscosity in Liquid State

Kinematic viscosity was determined by analysing the damped torsional oscillations of a BeO vessel (with an inner diameter of 13 mm) containing the metallic melt during heating (up to 1700 °C) and during subsequent slow cooling. A working chamber was

initially evacuated to 0.001 Pa, and then it was filled with helium to a pressure of 10^5 Pa. The measurements were performed during isothermal holding (for at least 5 min), with stepwise changes in temperature of 20–30 °C. The temperature was maintained constant with an accuracy of 1 °C using a precision controller (optical pyrometer). During the measurements, oscillation parameters were monitored optically, using an automatic system for photo-recording of oscillation. The measurement and experimental data treatment procedures are described in [32,33].

2.4. Measurement of the Electrical Resistivity in Liquid State

The electrical resistivity of the $Fe_{48}Cr_{15}Mo_{14}C_{15}B_6Y_2$ liquid was measured by using the rotating magnetic field method during heating (up to 1700 °C) and subsequent cooling. A working chamber was initially evacuated to 0.001 Pa, and then filled with helium to a pressure of 10^5 Pa. Samples were held in this chamber for 5–8 min at the melting temperature and then heated up to 1700 °C in increments of 30–50 °C. Isothermal holding at the measurement points was not less than 10 min. The electrical resistivity was measured as described in [34,35].

2.5. Measurement of the Density in Liquid State

The density of liquid metal upon heating up to 1760 °C and subsequent cooling was measured by the sessile drop method [20]. The test sample of a given mass and volume (about 1 cm^3) was placed on a horizontal fireproof backplate made of BeO. This was placed into an electric furnace. The working chamber was preliminarily evacuated to a pressure of 0.001 Pa. Helium was then pumped in until a pressure of 10^5 Pa was achieved. This was done to protect the sample from air contamination and boiling up. The sample was heated until an ellipse-shaped melt drop resting on the horizontal backplate was formed. Isothermal holding at the measurement points was at least 5 min. The samples were held in the chamber with an inert atmosphere at the melting temperature for 5–8 min and were then heated up to 1800 °C in increments of 30–50 °C. The drop profile was recorded with a digital camera. The drop images were then transferred to a computer. In order to calculate the drop's volume, the geometric parameters of the drop's contours were measured from the images obtained during the experiment using the SIAMS 700 image analysis software package (SIAMS, Yekaterinburg, Russia). The density rate for the liquid state was obtained as described in [36]. The absolute error of determining the melt density did not exceed 5%. A detailed methodology of the procedure performed is described in [37].

3. Results and Discussion

In this study, $Fe_{48}Cr_{15}Mo_{14}C_{15}B_6Y_2$ alloys with both amorphous and crystalline phases were produced. This was confirmed through XRD analysis, SEM imaging, and microhardness measurements. Figure 1 shows the SEM images of the middle area of an alloy ingot. Several inclusions, in the form of dendric structures (see Figure 1a) and microinclusions (see Figure 1b,c), were found within the sample. Through microhardness analysis, it was determined that the dendritic matrices were composed of ledeburite, having microhardness values of about 1300–1350 HV, whilst the microinclusios were composed of complex carbides containing Mo and Fe, having a microhardness of about 2100–2300 HV. The microhardness result, obtained by investigation of ledeburite and carbides, is very close to literature data for cast iron, steel alloy, and amorphous films [38–40].

X-Ray analysis of the as-cast sample confirmed that the sample is in an amorphous-crystalline state (see the amorphous halo in Figure 1d). The determined crystalline volume fraction reached approximately 30%. Moreover, analysis shows that carbides structures are similar to the Fe_3Mo_3C composition.

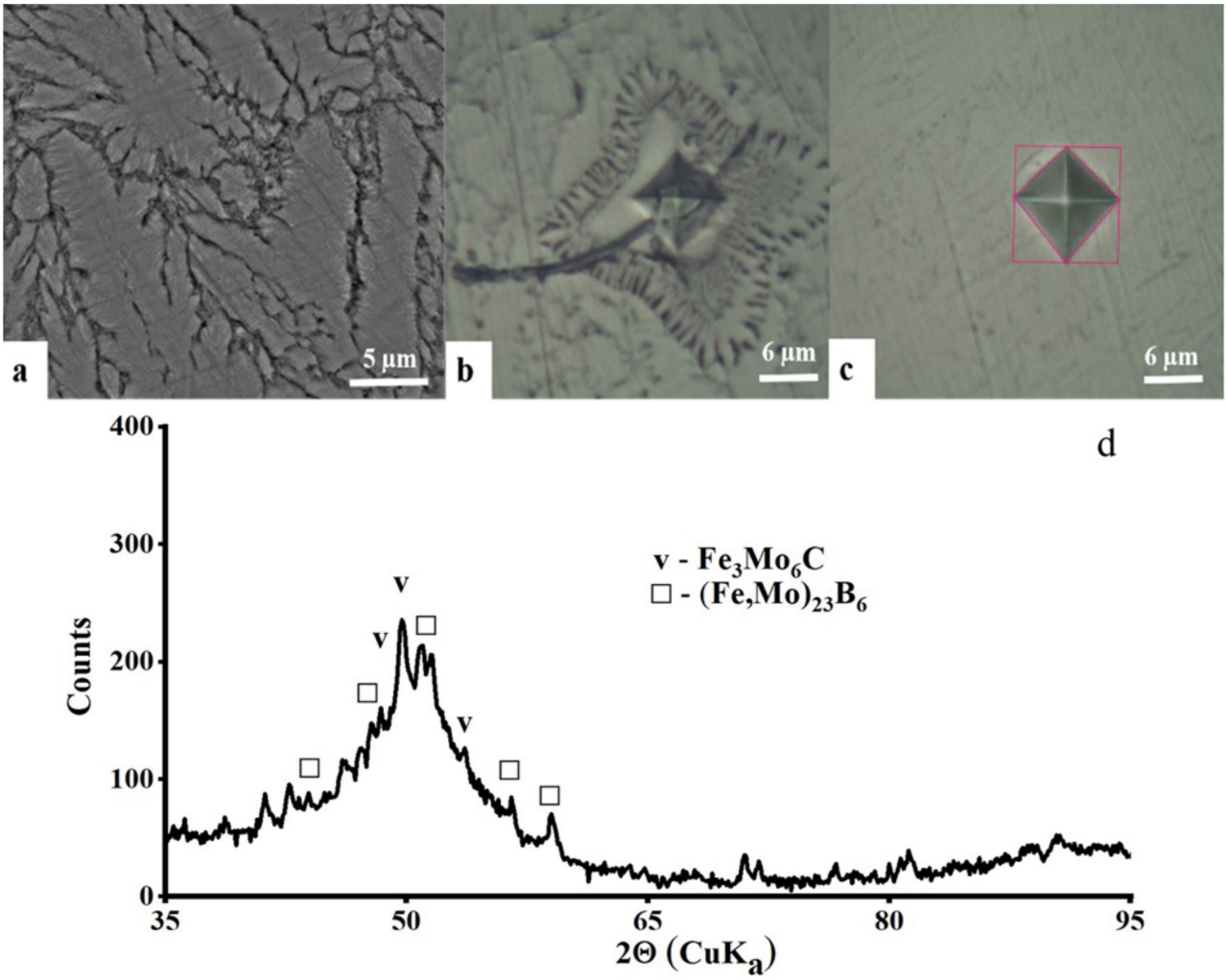

Figure 1. Microstructure of $Fe_{48}Cr_{15}Mo_{14}C_{15}B_6Y_2$ alloy in the middle area of the sample of 12 mm in diameter: (**a**) dendrite structure; (**b**,**c**) microhardness of the selected carbide phase and dendrite matrix, respectively. (**d**) XRD pattern of the as-cast sample.

It should also be noted that the occurrence of an amorphous and crystalline phase in the as-cast sample was confirmed by the SEM analysis (Figure 2). It is observed that the sample has amorphous and crystalline phases (Figure 2a,b). Crystallite particles are distribute in an amorphous matrix and have a dendrite structure (Figure 2c,d). It should also be noted that the obtained SEM results are in a good agreement with the XRD analysis (Figure 1d).

A number of physical properties of the alloy in the liquid state were also successfully measured and are discussed below. During the measurements of these physical properties, no evidence of melt evaporation or loss in mass of the sample was observed.

3.1. Kinematic Viscosity

From the literature, it is known that for homogeneous melts, the viscous flow decreases with increasing temperature [41]. However, micro-inhomogeneities transferred from solid state may be present in metallic melts. These micro-inhomogeneities are specific for each melt and can persist for a long time [41]. The presence of micro-inhomogeneities can be evaluated from the heating and cooling curves for some structure-sensitive property of the melt (most frequently from its viscosity). By heating above the temperature of homogeneity, the melt irreversibly converts to a true solution state, which produces significant changes in the metal solidification conditions [41].

In this study, we measured the temperature-dependent kinematic viscosity of the $Fe_{48}Cr_{15}Mo_{14}C_{15}B_6Y_2$ alloy, whose cast structure consisted of two phases: a crystalline phase and an amorphous one as discussed above. An increase in viscosity for the $Fe_{48}Cr_{15}Mo_{14}C_{15}B_6Y_2$ alloy was observed in the temperature range of 1360 to 1550 °C (Figure 3a). This unusual increase in viscosity may be attributed to the fragmentation of the dendritic microstructure of the alloy and the formation of fragments in the volume of the BeO crucible. Another factor that may be responsible for such an increase in viscosity is the transformation of the amorphous phase to a crystalline one.

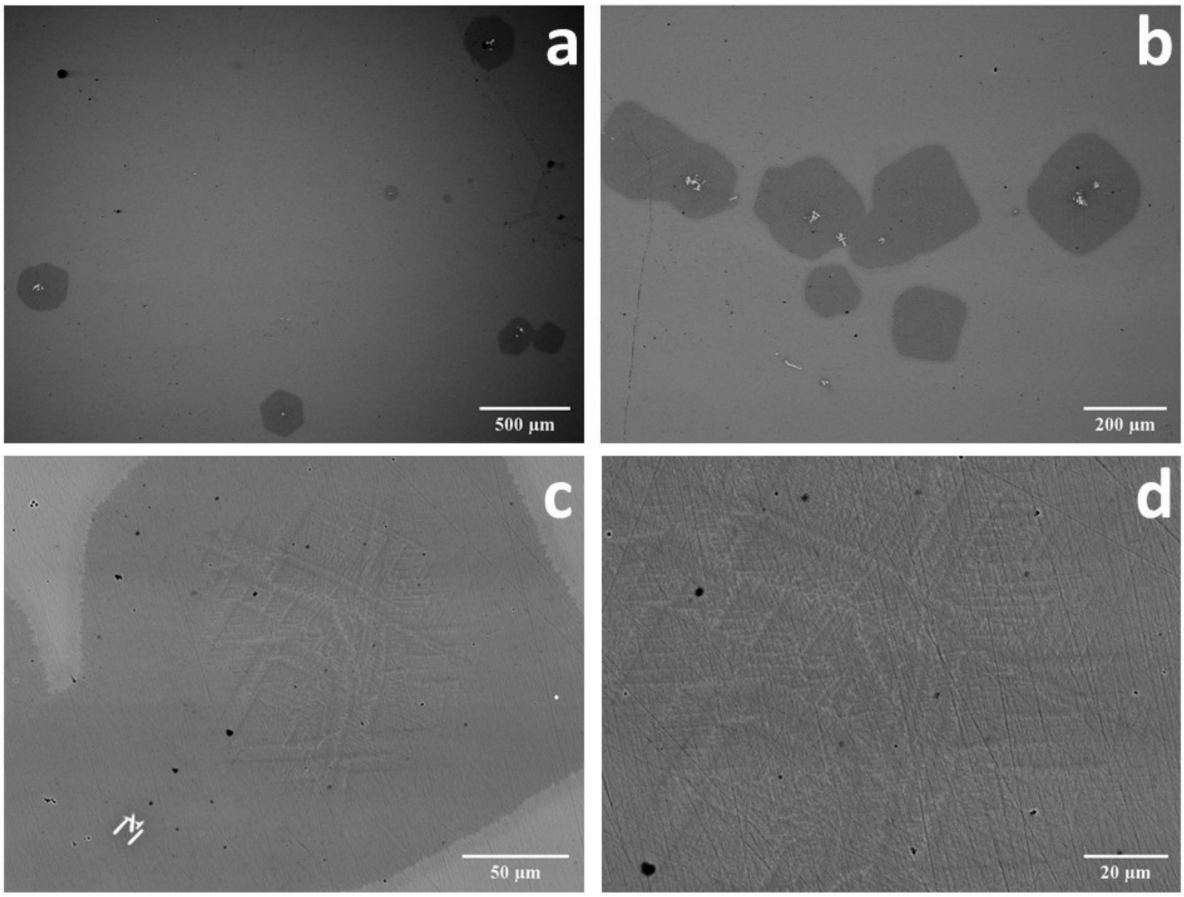

Figure 2. Scanning electronic microscopy of the as-cast $Fe_{48}Cr_{15}Mo_{14}C_{15}B_6Y_2$ alloy sample: (**a**,**b**) crystallites in amorphous matrix, (**c**,**d**) dendrite structure of crystals.

When the temperature exceeded 1550 °C we observed a sudden increase in the viscosity (Figure 3a), which is characteristic of the transition from a solid to a liquid state. The viscosity was then observed to decrease with increasing temperature within the temperature range of 1570 to 1650 °C (Figure 3a). After homogenization at 1650 °C, the viscosity of the metallic melt increased from 1510 to 1450 °C (Figure 3a). When the temperature of the sample was below its melting point of 1310 °C, the melt began to transition from the liquid state to a crystalline phase, avoiding amorphization.

The temperature-dependent kinematic viscosity of the $Fe_{48}Cr_{15}Mo_{14}C_{15}B_6Y_2$ sample after a repeated heating–cooling cycle is shown in Figure 3b. In this case, the temperature of homogenization was achieved during the first heating cycle. This was followed by slow cooling to the temperature of crystallization. Thus, in this instance, one expects no significant differences between subsequent heating and cooling cycles. Nonetheless, such measurements can provide additional information on the state of the liquid phase at high temperatures. As shown in Figure 3b, the liquid state in this heating cycle was achieved at 1380 °C. Increasing the temperature to 1570 °C led to a decrease in the melt

viscosity. Heating above this temperature resulted in a sudden increase in the viscous flow of the melt up to a temperature of 1590 °C, after which the viscosity started to decrease again (Figure 3b). Above 1300 °C, the alloy is in a liquid state. Equilibrium melt obeys the Arrhenius equation, i.e., the viscosity decreases with increasing temperature. At the stage of the first heating to 1560 °C, the melt is in a nonequilibrium state. Low viscosity corresponds to the flow of large clusters. An almost linear slight increase in viscosity at the stage of the first heating to 1560 °C corresponds to a slow detachment of atoms from clusters, i.e., reducing their average size. A sharp increase in viscosity corresponds to the decomposition of clusters and the transition of the melt to an equilibrium state. This state confirms the typical dependence of viscosity on temperature.

Figure 4 is showing the DSC curves of the as-cast sample. It is clearly seen that the crystallization and phase transformation processes started at about 600 °C and the melting process has started at above 1100 °C. Unfortunately, the characteristic property of DSC equipment did not allow us to heat up the sample above the 1400 °C, therefore it was impossible to obtain the melting of the whole volume of it. However, several phases were partly melted (approximately, with two different composition). On the cooling DSC curves (Figure 4), the crystallization of two phases (two crystallization peaks) is also clearly seen.

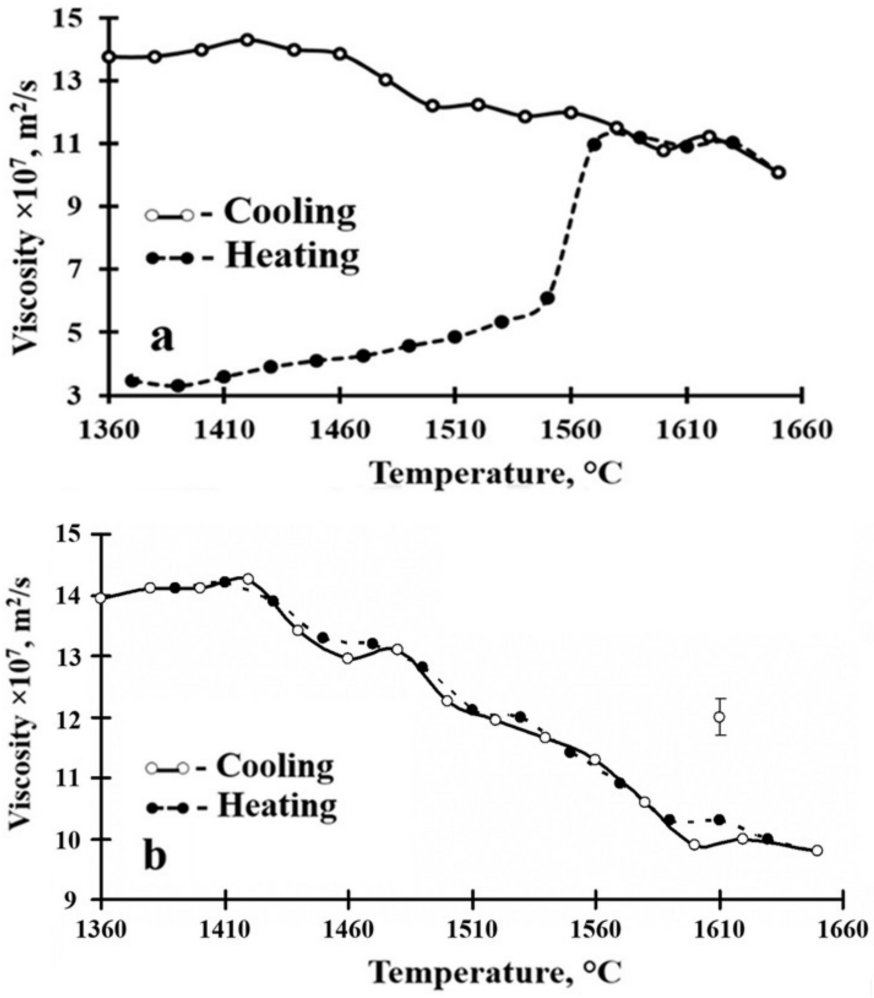

Figure 3. Viscosity of $Fe_{48}Cr_{15}Mo_{14}C_{15}B_6Y_2$ alloy at various temperatures: (**a**) the first measurement from the die-cast state; (**b**) the second measurement of the same sample after homogenization at 1650 °C (repeated).

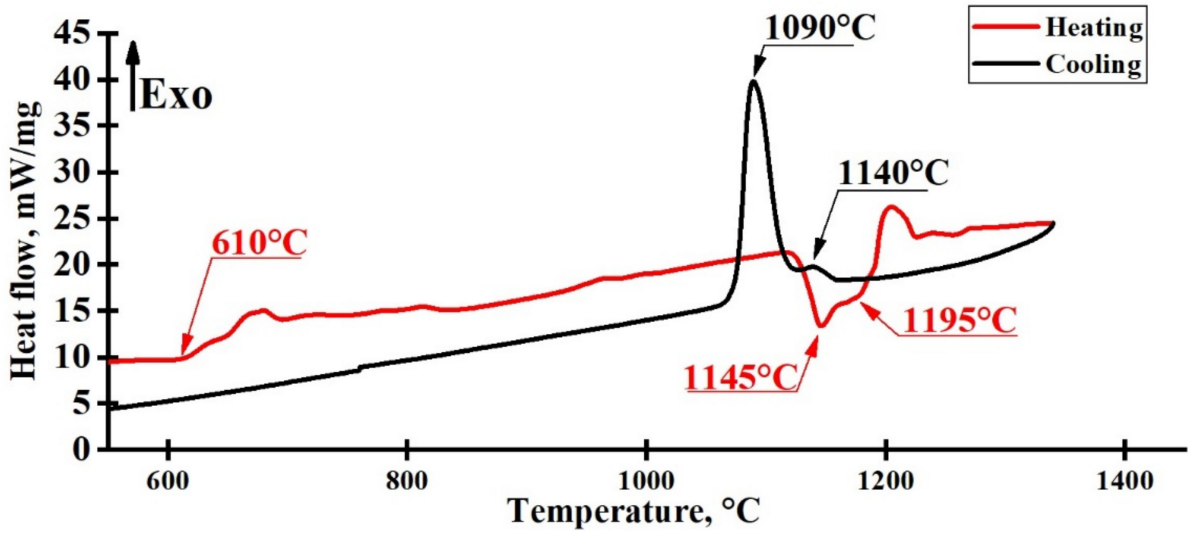

Figure 4. DSC curves of the as-cast alloy.

The microstructure of the $Fe_{48}Cr_{15}Mo_{14}C_{15}B_6Y_2$ alloy, which was obtained after the second heating/cooling cycle, is shown in Figure 5a. This micrograph clearly shows that the alloy melt has recrystallized into a fine dispersed phase. Microhardness measurements indicated the presence of ledeburite (1490–1550 HV) and separated inclusions of complex carbides ($M_{23}C_6$ and M_6C) (2200–2500 HV). Furthermore, X-ray diffraction of the sample revealed the presence of two phases, i.e., $Cr_{21.34}Fe_{1.66}C_6$ and Fe_3Mo_3C (Figure 5b). Thus, we can conclude that the cast structure of alloy after recrystallization from the liquid state corresponded to the structure of the high-alloy chilled cast iron.

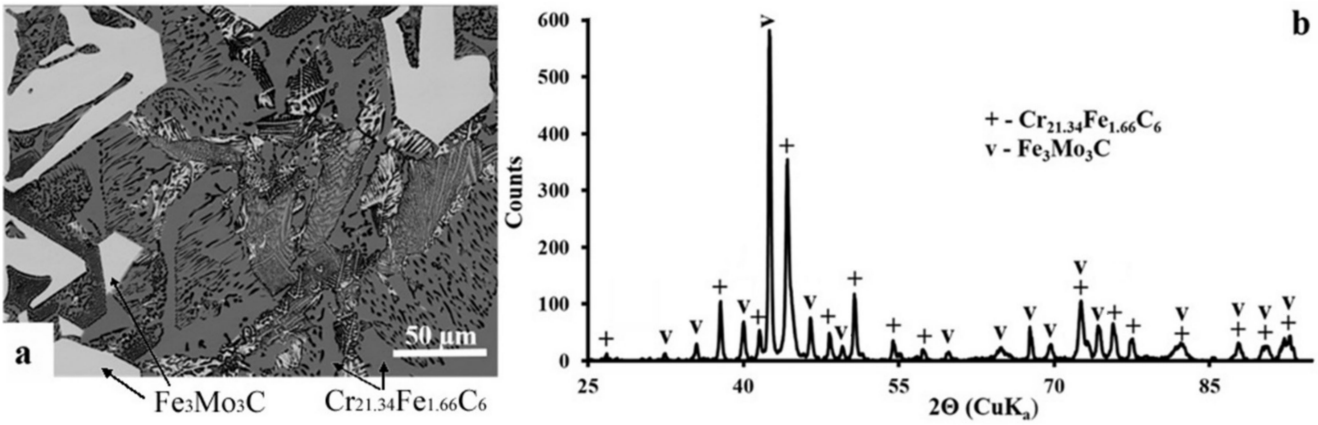

Figure 5. Microstructure of $Fe_{48}Cr_{15}Mo_{14}C_{15}B_6Y_2$ alloy after recrystallization from the liquid state: (**a**) the eutectic (ledeburite) structure containing complex carbides of types $M_{23}C_6$ and M_6C in it; (**b**) X-ray diffraction pattern of the same sample. The sample is presented here after the viscosity measurement.

3.2. Electrical Resistivity

The electrical resistivity of the $Fe_{48}Cr_{15}Mo_{14}C_{15}B_6Y_2$ alloy produced in this study was measured within the temperature range from 1200 to 1700 °C. The electrical resistivity was observed to decrease with increasing temperature, as shown in Figure 6. No obvious deviations were observed on the heating/cooling polytherms at 1580 and 1600 °C, the temperature ranges where an increase/decrease in kinematic viscosity was observed for heating and cooling, respectively. This indicates that electrical resistivity methods lack sensitivity when observing the changes occurring in the liquid state at these temperatures. The decrease in electrical resistivity with increasing temperature may be explained through

the microheterogeneous structure of metallic melts [32–47]. Melting of a multiphase cast iron ingot does not lead to the immediate formation of a homogeneous solution of the alloying elements in iron, with a microheterogeneous state persisting within a certain temperature range. The temperature corresponding to the irreversible transition of the melt into a homogeneous state may be determined from the high-temperature coinciding portion of the heating and cooling polytherms. This was found to be close to 1700 °C (Figure 6) for the $Fe_{48}Cr_{15}Mo_{14}C_{15}B_6Y_2$ alloy produced in this study when using electrical resistivity measurements.

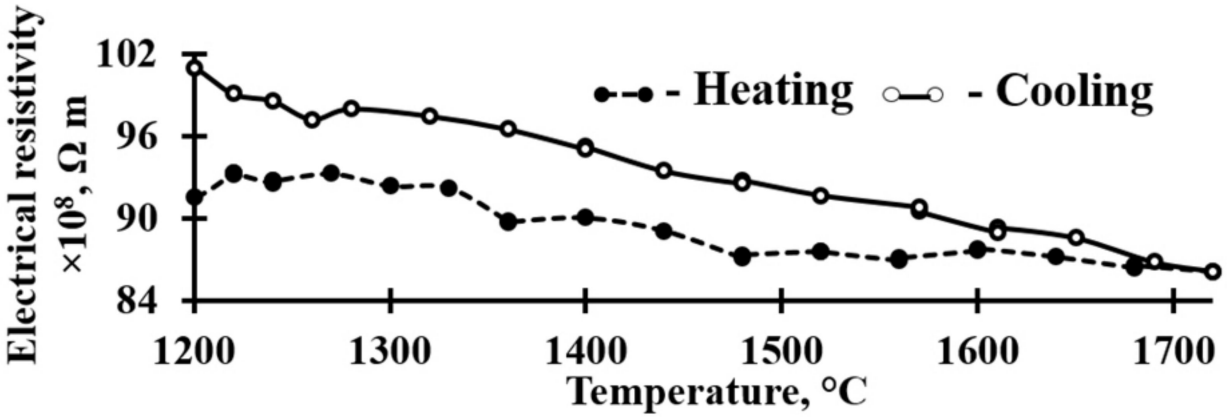

Figure 6. Electrical resistivity of $Fe_{48}Cr_{15}Mo_{14}C_{15}B_6Y_2$ alloy in the liquid state at various temperatures.

3.3. Density

Figure 7 shows how the density and shape of a drop of the $Fe_{48}Cr_{15}Mo_{14}C_{15}B_6Y_2$ alloy produced in this study change when the temperature is increased up to 1800 °C. During the first heating cycle, the density of the sample changed slightly with heating (7.03–7.07 g/cm^3). However, during the first cooling cycle, larger changes in the density were recorded (Figure 7a). This may be explained by the fact that when the temperature of homogenization is achieved, the alloy drop is cleaned from any film that may be present on its surface.

The heredity of the cast state for the examined sample was destroyed at 1800 °C and the behaviour of the liquid state upon cooling from 1800 to 1260 °C corresponded to the formation of another type of alloy, such as a high-alloy chilled cast iron. This means that the nucleation and growth of the crystalline phase, mainly the carbide phases, upon crystallization are accompanied with a decrease in volume of the sessile drop in the liquid state. As a result of this transition, the density of the metallic melt is increased (Figure 7a). The density of the sessile drop at 1260 °C was 7.43–7.48 g/cm^3. The repeated measurement of density for this sessile drop showed that the heating and cooling curves were coincident in the wide range of temperature from 1310 to 1700 °C (Figure 7b). This confirms that the transitions in the liquid phase do not have a significant effect on the density after the process of recrystallization. However, some oscillations in density were observed in the heating curve from 1260 to 1310 °C (Figure 7b). These oscillations were due to the destruction of the film on the surface of the sessile drop (Figure 7b). As a general observation, one may conclude that the density of the $Fe_{48}Cr_{15}Mo_{14}C_{15}B_6Y_2$ alloy decreases with increasing temperature.

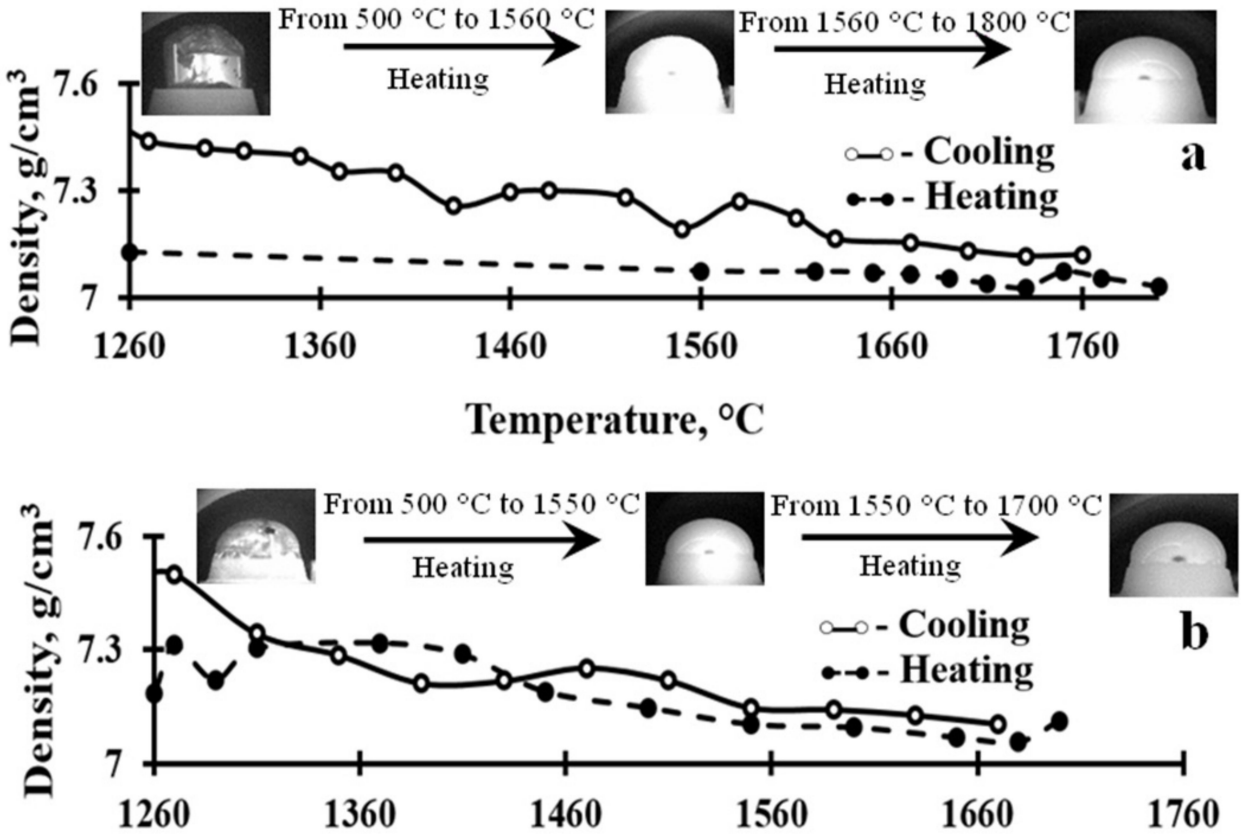

Figure 7. Density of $Fe_{48}Cr_{15}Mo_{14}C_{15}B_6Y_2$ alloy in the liquid state at various temperatures: (**a**) the first measurement from the die-cast state; (**b**) the second measurement of the same sample after homogenization at 1800 °C (repeated). Inserted photos (**a**,**b**) show changes in the sessile drop during the heating–cooling process in a wide temperature range.

4. Conclusions

The thermophysical properties (viscosity, electrical resistance, and density) of a $Fe_{48}Cr_{15}Mo_{14}C_{15}B_6Y_2$ bulk amorphous-crystalline alloy at high temperatures were studied. Viscosity measurements gave the most complete picture of the processes taking place in the liquid state of the alloy studied. In fact, only viscosity measurements showed a possible change in the structure of the liquid within the temperature range of 1580 and 1600 °C, whereby the viscous flow of metallic melts was extremely increased. Furthermore, it was confirmed that the density and electrical resistivity of $Fe_{48}Cr_{15}Mo_{14}C_{15}B_6Y_2$ alloy in the liquid state tend to decrease with increasing temperature.

Author Contributions: Conceptualization, V.S.T. and D.S.K.; methodology and validation, V.V.K. and V.V.V.; software, A.I.B.; formal analysis, A.R.K. and A.A.T.; investigation, V.Y.Z.; resources, A.I.B., V.Y.Z., V.S.T. and J.F.M.V.I.; data curation, V.S.T. and J.F.M.V.I.; writing—original draft preparation, D.S.K. and A.R.K.; writing—review and editing, A.R.K. and V.Y.Z.; visualization, A.R.K. and D.S.K.; supervision, V.S.T. and J.F.M.V.I.; project administration, J.F.M.V.I.; funding acquisition, J.F.M.V.I. All authors have read and agreed to the published version of the manuscript.

Funding: This research was funded by of the Ministry of Science and Higher Education of the Russian Federation in the framework of the Increase Competitiveness Program of NUST «MISiS» (grant number K2-2020-046). V.S.T., V.V.K. and V.V.V gratefully acknowledge the financial support made within the framework of state work No. FEUZ-0836-0020. Also, D.S.K. and J.V.I. gratefully acknowledge the European Union's Horizon 2020 research and innovation programme under the Marie Skłodowska-Curie grant agreement No. 897815 NanoSurf.

Institutional Review Board Statement: Not applicable.

Informed Consent Statement: Not applicable.

Data Availability Statement: The data presented in this study are available on request from the corresponding author.

Conflicts of Interest: The authors declare no conflict of interest.

References

1. Inoue, A.; Shinohara, Y.; Gook, J.S. Thermal and Magnetic Properties of Bulk Fe-Based Glassy Alloys Prepared by Copper Mold Casting. *Mater. Trans. JIM* **1995**, *36*, 1427–1430. [CrossRef]
2. Shen, T.D.; Schwarz, R.B. Bulk ferromagnetic glasses in the Fe-Ni-P-B system. *Acta Mater.* **2001**, *49*, 837–850. [CrossRef]
3. Buschow, K.H.J. *Formation, Structure, Properties, and Applications. Handbook of Magnetic Materials*; Elsevier: Amsterdam, The Netherlands, 2013; Volume 21, pp. 131–171.
4. Li, X.; Shi, Z.; Zhang, T. Effect of similar element substitution on Fe-B-Si-Mo bulk metallic glasses studied by experiment and ab initio molecular dynamics simulation. *J. Alloys Compd.* **2019**, *5*, 1139–1144. [CrossRef]
5. Pang, S.J.; Zhang, T.; Asami, K.; Inoue, A. Bulk glassy Fe–Cr–Mo–C–B alloys with high corrosion resistance. *Corros. Sci.* **2002**, *44*, 1847–1856. [CrossRef]
6. Yao, J.H.; Wang, J.Q.; Li, Y. Ductile Fe–Nb–B bulk metallic glass with ultrahigh strength. *Appl. Phys. Lett.* **2008**, *92*, 251906. [CrossRef]
7. Shi, M.J.; Pang, S.J.; Zhang, T. Towards improved integrated properties in FeCrPCB bulk metallic glasses by Cr addition. *Intermetallics* **2015**, *61*, 16–20. [CrossRef]
8. Ponnambalam, V.; Poon, S.J.; Shiflet, G.J. Synthesis of iron-based bulk metallic glasses as nonferromagnetic amorphous steel alloys. *J. Mater. Res.* **2004**, *19*, 3046–3053. [CrossRef]
9. Lu, Z.P.; Liu, C.T.; Porter, W.D. Role of yttrium in glass formation of Fe-based bulk metallic glasses. *Appl. Phys. Lett.* **2003**, *83*, 2581–2583. [CrossRef]
10. Louzguine-Luzgin, D.V.; Bazlov, A.I.; Ketov, S.V.; Greer, A.L.; Inoue, A. Crystal growth limitation as a critical factor for formation of Fe-based bulk metallic glasses. *Acta Mater.* **2015**, *82*, 396–402. [CrossRef]
11. Wan, C.; Yang, W.; Liu, H.; Zuo, M.; Li, Q.; Ma, Z.; Zhao, Y.; Inoue, A. Ductile Fe-based bulk metallic glasses at room temperature. *Mat. Sci. Technol.* **2018**, *34*, 751–756. [CrossRef]
12. Li, H.X.; Lu, Z.C.; Wang, S.L.; Wu, Y.; Lu, Z.P. Fe-based bulk metallic glasses: Glass formation, fabrication, properties and applications. *Prog. Mater. Sci.* **2019**, *103*, 235–318. [CrossRef]
13. Lu, Y.; Huang, Y.; Shen, J.; Lu, X.; Qin, Z.; Zhang, Z. Effect of Co addition on the shear viscosity of Fe-based bulk metallic glasses. *J. Non-Cryst. Solids* **2014**, *403*, 62–66. [CrossRef]
14. Takeuchi, A.; Inoue, A. Analyses of glass-transition behavior of Pd-based metallic glass with linear solution to non-linear differential equation. *Mater. Sci. Eng. A* **2007**, *449*, 594–598. [CrossRef]
15. Blodgett, M.; Egami, T.; Nussinov, Z.; Kelton, K.F. Unexpected Universality in the Viscosity of Metallic Liquids. Available online: https://arxiv.org/abs/1407.7558v1 (accessed on 30 March 2021).
16. Bitoh, T.; Watanabe, D. Effect of Yttrium Addition on Glass-Forming Ability and Magnetic Properties of Fe–Co–B–Si–Nb Bulk Metallic Glass. *Metals* **2015**, *5*, 1127–1135. [CrossRef]
17. Khalifa, H.E.; Cheney, J.L.; Vecchio, K.S. Effect of Mo–Fe substitution on glass forming ability, thermal stability, and hardness of Fe–C–B–Mo–Cr–W bulk amorphous alloys. *Mater. Sci. Eng. A* **2008**, *490*, 221–228. [CrossRef]
18. Hidal, K.; Sekido, N.; Perepezko, J.H. Critical cooling rate for Fe48Cr15Mo14Y2C15B6 bulk metallic glass formation. *Intermetallics* **2006**, *14*, 898–902. [CrossRef]
19. Han, J.; Wang, C.; Kou, S.; Liu, X. Thermal stability, crystallization behavior, Vickers hardness and magnetic properties of Fe–Co–Ni–Cr–Mo–C–B–Y bulk metallic glasses. *Trans. Nonferrous Met. Soc. China* **2013**, *23*, 148–155. [CrossRef]
20. Baser, T.; Baricco, M. Fe-based bulk metallic glasses with Y addition. *J. Alloys Compd.* **2007**, *176*, 434–435. [CrossRef]
21. Amiya, K.; Inoue, A. Fe-(Cr, Mo)-(C, B)-Tm Bulk metallic glasses with high strength and high glass-forming ability. *Mater. Transac.* **2008**, *18*, 1615–1618. [CrossRef]
22. Filippov, K.S. Correlation between Hereditary Structures and Properties of an Fe50Cr15Mo14C15B6 Bulk Amorphous Alloy in the Solid and Liquid States. *Russ. Metall. Met.* **2010**, *5*, 379–383. [CrossRef]
23. Li, Y.; Li, R.; Pang, S.; Chen, B.; Georgarakis, K.; Le Moulec, A.; Vaughan, G.; Zhang, T.; Yavari, A.R. Investigation of viscosity and crystallization in supercooled-liquid region of Zr-based glassy alloys. *J. Non-Cryst. Solids* **2012**, *358*, 150. [CrossRef]
24. Csach, K.; Bobrov, O.P.; Khonik, V.A.; Lyakhov, S.A.; Kitagawa, K. Relationship between the shear viscosity and heating rate of metallic glasses below Tg. *Phys. Rev. B* **2006**, *73*, 092107. [CrossRef]
25. Liu, B.B.; Liu, B.Y.; Fang, X.S.; Zhang, L.Q.; Ye, F.; Chen, G.L. Viscosity of Zr55Cu30Al10Ni5 bulk metallic glass measured by laser viscometer. *J. Alloys Compd.* **2010**, *504*, S208–S210. [CrossRef]
26. Yokoyama, Y.; Tokunaga, H.; Yavari, A.R.; Yamada, M.; Yamasaki, T.; Fujita, K.; Inoue, A. Viscous flow in sliding shear band formed during tensile deformation of hypoeutectic Zr-based metallic glass. *Intermetallics* **2011**, *19*, 1683–1687. [CrossRef]
27. Evenson, Z.; Schmitt, T.; Nicola, M.; Gallino, I.; Busch, R. High temperature melt viscosity and fragile to strong transition in Zr–Cu–Ni–Al–Nb (Ti) and Cu 47 Ti 34 Zr 11 Ni 8 bulk metallic glasses. *Acta Mater.* **2012**, *60*, 4712–4719. [CrossRef]

28. Evenson, Z.; Busch, R. Enthalpy recovery and free volume relaxation in a Zr44Ti11Ni10Cu10Be25 bulk metallic glass. *J. Alloys Compd.* **2011**, *509*, S38–S41. [CrossRef]
29. Lu, Y.Z.; Huang, Y.J.; Zheng, W.; Shen, J. Free volume and viscosity of Fe–Co–Cr–Mo–C–B–Y bulk metallic glasses and their correlation with glass-forming ability. *J. Non-Cryst. Solids* **2012**, *358*, 1274–1277. [CrossRef]
30. Pilarczyk, W.; Nowosielski, R.; Januszka, A. Structure and properties of Fe-Cr-Mo-C bulk metallic glasses obtained by die casting method. *J. Achiev. Mater. Manuf. Eng.* **2010**, *42*, 81–87.
31. Shelekhov, E.V.; Sviridova, T.A. Modeling of the Motion and Heating of Balls in a Planetary Ball Mill: Effect of Processing Conditions on the Mechanical Activation Products of Ni + Nb Powder Mixtures. *Materialovedenie* **1999**, *10*, 13–22. (In Russian)
32. Konashkov, V.V.; Tsepelev, V.S.; V'yukhin, V.V.; Povodator, A.M.; Podol'skaya, A.I. A computer-aided plant for studying the kinematic viscosity of high-temperature metallic melts. *Instrum. Exp. Technol.* **2011**, *54*, 284–285. [CrossRef]
33. Povodator, A.M.; Konashkov, V.V.; V'yukhin, V.V.; Tsepelev, V.S. A Method for Determining the Damping Rate for Non-Contact Measurement of Viscosity of High-Temperature Metallic Melts. RF Patent 2386948, 20 April 2010.
34. Tyagunov, G.V. The measurement of the resistivity by the rotating magnetic field method. *Zavod. Labor.* **2003**, *69*, 36. [CrossRef]
35. Konashkov, V.V.; Povodator, A.M.; V'yukhin, V.V.; Tsepelev, V.S. Method of Measuring the Electrical Resistance of Metallic Melts by the Rotating Magnetic Field Method. RF Patent 2457473, 27 July 2012.
36. Tsepelev, V.V.; Vyukhin, V.V.; Povodator, A. The unit for determining the density and surface tension of metallic liquid alloys, using the sessile drop method. *Mater. Sci. Forum* **2017**, *889*, 108–112. Available online: https://www.scientific.net/MSF.889.108 (accessed on 30 March 2021). [CrossRef]
37. Koshevnik, A.Y.; Kusakov, M.M.; Lubman, N.M. Change in the Surface Tension from the Sessile Drop Sizes. *Zh. Fiz. Khim.* **1953**, *12*, 1886.
38. Shveev, I.A. Displaying structural property and inheritance of cast iron surfacing on steel base. *IOP Conf. Ser. Mater. Sci. Eng.* **2016**, *134*, 012037. [CrossRef]
39. Ghidelli, M.; Volland, A.; Blandin, J.J.; Pardoen, T.; Raskin, J.P.; Mompiou, F.; Djemia, F.; Gravier, S. Exploring the mechanical size effects in Zr65Ni35 thin film metallic glasses. *J. Alloys Compd.* **2014**, *615*, S90–S92. [CrossRef]
40. Ghidelli, M.; Gravier, S.; Blandin, J.J.; Djemia, F.; Mompiou, F.; Abadias, G.; Raskin, J.P.; Pardoen, T. Extrinsic mechanical size effects in thin ZrNi metallic glass films. *Acta Mater.* **2015**, *90*, 232–241. [CrossRef]
41. Chikova, O.A.; Il'in, V.Y.; Tsepelev, V.S.; V'yukhin, V.V. Viscosity of high-entropy melts in the Cu—Bi—Sn—In—Pb system. *Inorg. Mater.* **2016**, *52*, 517. [CrossRef]
42. Ostrovskii, O.A.; Grigoryan, V.A.; Vishkarev, A.F. Properties of Metallic Melts (Metallurgiya, Moscow, 1988). (in Russian)
43. Popel, P.S.; Chikova, O.A.; Matveev, V.M. Metastable Colloidal States of Liquid Metallic Solutions. *High. Temp. Mater. Proc.* **1995**, *14*, 219–233. [CrossRef]
44. Wang, J.; He, S.; Sun, B.; Guo, Q.; Nishio, M. Grain refinement of Al–Si alloy (A356) by melt thermal treatment. *J. Mater. Proc. Technol.* **2003**, *141*, 29–34. [CrossRef]
45. Morris, J.R.; Dahlborg, U.; Calvo-Dahlborg, M. Recent development and outstanding challenges in theory and modeling of liquid metals. *J. Non-Cryst. Solids* **2007**, *353*, 3444–3453. [CrossRef]
46. Calvo-Dahlborg, M.; Popel, P.S.; Kramer, M.J.; Besser, M.; Morris, J.R. Superheat dependent microstructure of molten Al–Si alloys of different composition studied by small angle neutron scattering. *J. Alloys Compd.* **2013**, *550*, 9–22. [CrossRef]
47. Borovykh, M.A.; Chikova, O.A.; Tsepelev, V.S.; V'yukhin, V.V. Measurement of the electrical resistivity of liquid 32G2 and 32G1 steels by the rotating magnetic field method. *Russ. Metall. Met.* **2017**, *3*, 175–178. [CrossRef]